International Journal of Fatigue 130 (2020) 105283

Contents lists available at ScienceDirect

International Journal of Fatigue

journal homepage: www.elsevier.com/locate/ijfatigue

Residual stress relaxation and duty cycle on high cycle fatigue life of micro-arc oxidation coated AA7075-T6 alloy

Weibing Dai[a], Jin Hao[a], Changyou Li[a,*], David He[a,*], Dawei Jia[b], Yimin Zhang[c], Zhi Tan[d]

[a] School of Mechanical Engineering and Automation, Northeastern University, Shenyang, China
[b] AVIC SAC Commercial Aircraft Co., Ltd., Shenyang, China
[c] School of Institute of Equipment Reliability, Shenyang University of Chemical Technology, Shenyang, China
[d] Shenyang Machine Tool Co., Ltd., Shenyang, China

ARTICLE INFO

Keywords:
Micro-arc oxidation
Duty cycle
Residual stress relaxation
Fatigue

ABSTRACT

Ceramic coatings were produced on AA7075-T6 alloy by micro-arc oxidation (MAO). The MAO treatment was performed at different duty cycles (8, 10, 15, and 20%). Effects of duty cycle on microstructure and fatigue behavior of the coated samples were investigated. Surface features and cross-section morphology, and fatigue fracture were observed by SEM and laser microscope. Phase structure and residual stress in the coatings were analyzed by X-ray diffraction. The nature and relaxation mechanism of the residual stress were revealed. Finally, the influence of the residual stress relaxation on the fatigue life at high and low cyclic stresses was explored.

1. Introduction

Micro-arc oxidation (MAO) is a relatively new surface treatment technology with broad range of application prospects. Light materials treated by MAO coating technology exhibit excellent wear resistance and high corrosion resistance [1,2]. Moreover, MAO had potential application value in medicine and can serve as a surface treatment process for human implants [3]. In addition to the excellent abrasion resistance and anti-corrosive property, the microscale gouges, sub-microscale pores, and beneficial phase components of the coatings are also the reasons for the extensive utilization of MAO technology in human implants. Aluminum (Al) alloy is increasingly used in automotive and aerospace industries [4]. Importantly, the materials used in these fields should exhibit excellent fatigue performance and extraordinary corrosion resistance property [5]. Moreover, fatigue behavior is the key parameters of aviation material testing. Although hardness, wear resistance, and corrosion resistance of the coated Al alloy surface can be improved after MAO treatment [6], the fatigue performance still remained inferior [7–10]. Residual tensile stress induced into the substrate covered with thick coating results in the decrease of fatigue life of MAO coated Al alloy. Before the advent of MAO treatment, shot peening technology produced residual compressive stress in the Al alloy substrate and improved the fatigue performance of the coated samples compared to that of the samples treated only by MAO [9,11–14]. However, some researchers indicated that the residual stress was not the main factor decreasing the fatigue life of the substrate after MAO treatment [10,15,16]. Thus, the mechanism of residual stress on coated samples needs to be further investigated. On the other hand, the MAO coatings consisted of the defects (pores, micro-cracks, and the scalloped oxide/titanium interface) that were prone to crack initiation, which impaired fatigue property of the substrate [10,14,16–18]. More importantly, studies showed that the crack originated from the MAO coating [10,15]. Therefore, Wang et al. [19] sealed the MAO coating surface. The result of fatigue test indicated that fatigue life of the sealed samples was improved by 50% compared to that of bare Al alloy. These changes suggest that the micro-pores and thermal cracks on the coating surface significantly influenced the fatigue life. Moreover, the fatigue behavior of sealed Al alloy specimens covered with MAO coating under corrosive environment were also improved [20]. Additionally, the polishing treatment of the interface made the fatigue behavior of the coated samples excellent [14,21]. The decrease in overgrowth of the coating into the substrate led to the result. It should be noted that the decrease in the fatigue life of the substrate with thin ceramic layers insignificant compared to the thick coating. Wasekar et al. [10] indicated the propagation of cracks may stagnate at the coating-substrate interface, which was attributed to the insignificant damage of fatigue behavior with the thin coating. Unfortunately, the impaired mechanism of the MAO thin film on the fatigue performance was not further explored.

Pulse power is an energy supply device commonly used in the MAO process. During the MAO process, duty cycle affected the surface quality and fatigue performance of coated samples. Most recent MAO

* Corresponding authors.
E-mail addresses: chyli@mail.neu.edu.cn (C. Li), davidhe@uic.edu (D. He).

https://doi.org/10.1016/j.ijfatigue.2019.105283
Received 3 August 2019; Received in revised form 14 September 2019; Accepted 16 September 2019
Available online 17 September 2019
0142-1123/

experiments on the duty cycle focused on growth and surface quality of ceramic coatings [22,23]. Weng et al. [22] reported that oxide film produced on Al by MAO treatment, with constant current density and a series of positive-pulse duty cycles ranging from 2 to 18%, had a maximum thickness and best section morphology at the 10% duty cycle. Moreover, the growth rate of the coatings increased gradually with decreasing duty cycle (10–80%) at frequency $f = 1000$ Hz [24]. Arunnellaiappan et al. [23] asserted that the ceramic coatings, with fine pore morphology, deposited on AA7075 were obtained by MAO at 1000 Hz frequency and 20% duty cycle. The coated samples exhibited high corrosion resistance. However, the above studies were carried out under the condition that thicker coatings were deposited on surface of light alloys. Effects of duty cycle on microstructure of thin MAO coatings and fatigue behavior of coated samples were rarely reported. At the initial stage of MAO treatment, studying the effect of duty cycles on the microstructure of the coatings can provide a reference for the study of MAO growth mechanism. Since reducing the impairment of coatings could increase fatigue life of coated samples, selection of an appropriate duty cycle is an important research topic. Moreover, the investigation of residual stress in MAO coating was significant for fatigue behavior of coated samples. In this study, 7075-T6 Al alloy was selected as the experimental material. In order to fabricate thinner ceramic layers, the MAO time was controlled within 24 min. The effect of duty cycles in the range from 8 to 20% on the microstructure of coatings was studied. Moreover, residual stress relaxation and its effect on fatigue behavior were further discussed. Meanwhile, the mechanism of the MAO coating on the fatigue performance of the coated 7075 Al alloy was revealed. The purpose of this study is to obtain a duty cycle with less damage to the fatigue property and reveal the mechanism of residual stress in the MAO coating affecting the high cycle fatigue life of the substrate.

2. Materials and methods

2.1. Coating preparation

The investigation in this study was conducted on the 7075-T6 Al alloy. The nominal chemical composition of the Al alloy is listed in Table 1. Mechanical properties were obtained by static tensile test, involving force loading (0.2 kN sec^{-1}) and displacement loading (0.07 mm sec^{-1}). The AA7075 was treated to the T6 condition that involved solution heat treatment, cold working, and artificial aging [7]. The parent plate was 1.6 mm thick AA7075 alloy (Ra = 0.8) supplied by Shenyang Aircraft Corporation, Liaoning Province, China. First, substrates were obtained by cutting the samples from parent plate using a wire cutting machine and these substrates were used for axial tensile–tensile fatigue testing. The specimen geometry is shown in Fig. 1. The side of the specimen was polished to Ra = 0.8. No further conventional machining was performed during the preparation of the specimen.

The surface of the substrate was cleaned with absolute ethanol and rinsed with deionized water. Mechanical properties of the AA7075-T6 alloy are as follows: $\sigma_b = 579$ MPa, $\sigma_{0.2} = 504$ MPa, and $\delta = 15.9\%$.

To ensure that samples with identical duty cycle were immersed at the same environmental condition, a circular hole (Φ8) was drilled on one side of each sample. Prior to MAO, all samples were cleaned with ethanol. Then fifteen samples were bolted to a copper plate mounted on the anode of the electrolytic bath, with stainless steel as a counter electrode, as shown in Fig. 2. The electrolyte consisted of alkaline silicate solution containing Na_2SiO_3 (6.0 g L^{-1}), NaOH (1.2 g L^{-1}), $(NaPO_3)_6$ (35.0 g L^{-1}), and Na_2WO_4 (6.0 g L^{-1}) in distilled water. A 120 kW MAO device was utilized for the coating deposition. During the experiments, voltage waveforms and main pulse parameters, such as voltage amplitude, frequency, and duty cycle could be adjusted independently.

All oxide coatings were fabricated at a constant voltage of 550 V and frequency of 600 Hz with different duty cycles of 8, 10, 15, and 20% for 24 min. Consequently, the current density varied with the duration of anodizing time. Sample codes and different process parameters used for each experiment are listed in Table 2.

The duty cycle is defined as:

$$D_t = [t_{on}/(t_{on} + t_{off})] \times 100\% \quad (1)$$

where t_{on} is the 'on' duration and t_{off} is the 'off' duration during a single cycle [24].

During the MAO process, the electrolyte temperature was controlled to remain below 50 °C using a cooling system. After MAO treatment, the coated samples were washed using water and dried using a blower.

2.2. Coating characterization

Coating thickness was measured using a scale in cross-section scanning electron microscopy (SEM) images of coated samples. Ten measurements were taken on the surface of each coated sample, and thickness was calculated by taking the average of the measurements. The measuring points were randomly selected within the range of CD in Fig. 1. Microstructure of the coatings and the cross-section morphology of the coated samples were examined by field emission SEM (FESEM, Ultra Plus, Carl Zeiss AG). Use carbon sputtering on the coating cross-section and its morphology was examined in the backscattered mode. Surface porosity of the coatings and distribution of the pores were analyzed by using ImageJ which was developed by the National Institutes of Health. The results were the average of the measurements. Surface porosity η was calculated by using Eq. (2) as follows.

$$\eta = \frac{S_0}{S} \times 100\% \quad (2)$$

where S_0 is the area of all micro-pores and S is the area of the SEM test area (area of SEM image).

Surface roughness of coatings was observed using a 3D measuring laser microscope (LEXT OLS4100). Phase composition of oxide films was investigated using a Philips X'Pert X-ray diffractometer (Cu–Kα radiation) operated at 40 kV and 40 mA and the scans were acquired at 2θ range from 20° to 80° with the scan speed of 1.5°/min and a step size in θ of 0.02°. However, the residual stress in MAO coating was analyzed by X-ray diffractometer (μ-x360s, Cr–Kα radiation, operated at 30 kV) and the Debye-Scherrer ring was acquired at incidence angle of 35.3°, diffraction angle of 138.75°, and in the (3 1 1) diffraction direction. Comparing the state of the Debye-Scherrer ring without and with residual stress can reflect the change in interplanar spacing. Thus, residual stress can be acquired. Five points on the coating surface of one sample was measured and the average was the residual stress. However, the measuring points of the residual stress should be away from the fracture for the samples after fatigue test.

2.3. Fatigue studies

The static tension and fatigue tests of the bare and MAO coated 7075-T6 Al alloy were carried out using a PC controlled EHF-EV200K2-

Table 1
Composition of 7075-T6 Al alloy.

Element	Cu	Si	Fe	Mn	Mg	Zn	Cr	Ti	Other	Al
Concentration	1.2–2.0	0.4	0.5	0.3	2.1–2.9	5.1–6.1	0.18–0.28	0.2	0.15	Balance

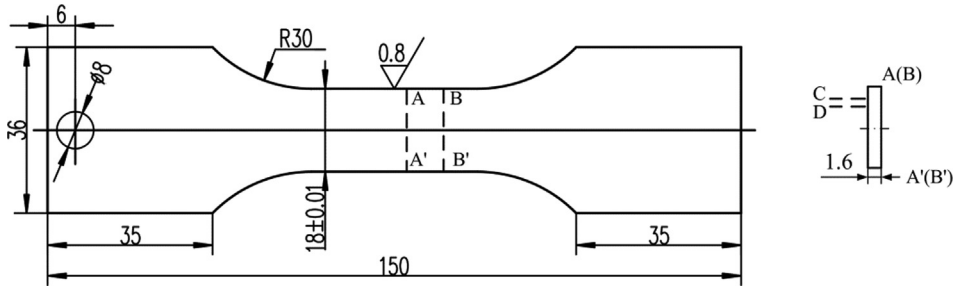

Fig. 1. The dimension (mm) of 7075-T6 Al alloy used in fatigue testing.

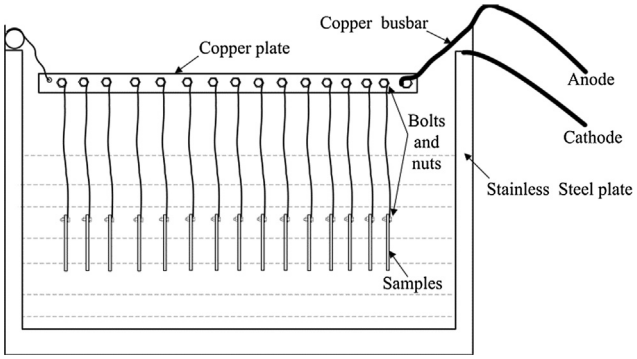

Fig. 2. Scheme experimental setup for the MAO treatment.

Table 2
Different process parameters used during the experiment for each sample.

Sample codes	Duty cycle (%)	Surface roughness Ra (μm)	Coating thickness (μm)	Surface porosity (%)	Elastic modulus (GPa)
a	8	0.544	5.0	6.08	76.1
b	10	0.592	5.3	5.83	75.6
c	15	0.717	7.4	7.08	75.2
d	20	0.68	7.3	4.49	74.2
Bare	–	–	–	–	71.9

040-1A machine. Fatigue tests were conducted at room temperature with a sinusoidal cycle of frequency ($f = 20$ Hz) and a stress ratio $R = 0.1$. Two cyclic maximum stress levels, based on the bare Al fatigue test data, were set as low cyclic stress (200 and 220 MPa) and high cyclic stress (350 and 410 MPa) at HCF regime, respectively. The fatigue life of these coated samples by MAO with different duty cycles were evaluated over a range of the cyclic maximum stress levels and compared with the fatigue life of each other and uncoated 7075-T6 Al alloy. Besides, considering the dispersion of the test data, three or four fatigue samples at each stress level were tested.

3. Results and discussion

3.1. Microstructure of coating

The surface morphologies of the oxide films formed on the 7075-T6 Al alloy substrate were observed by SEM. The SEM micrographs are shown in Fig. 3. The ceramic layers were formed at duty cycles of 8, 10, 15, and 20% for 24 min. Coating thickness was found to be in the range from 5.0 to 7.3 μm (Table 2). Table 2 summarizes that the thickness of the ceramic coatings increases with increasing duty cycle. However, the coating thickness of 20% duty cycle is close to that of 15% duty cycle. This is attributable to the fact that at the duty cycle of 20%, a huge energy input caused partially melted oxide films to splash into the electrolyte [22]. It should be noted that this results are not consistent with the conclusion by Zhang and his worker [25]. Zhang and his worker employed pulsed bipolar power supply to treat the high-phosphorus cast iron under constant voltage. With the increase of the duty cycles in ranged from 20 to 45%, the MAO coating thickness increased. However, the MAO treatment was conducted using DC pulsed unipolar power supply in this study. The difference in coating growth under different duty cycles is due to the cathode discharge. After a certain coating thickness had been reached, cathode discharge allowed the coating to grow [26]. In contrast, the coating depended on the low electrical resistance of the defects (mainly cracks) to form the discharge channel and grew without the cathode discharge. This can be seen from the presence of discharge pores in the cracks, as shown in Fig. 3. In addition, the surface porosity of the coatings hardly changes at the low duty cycles (8 and 10%), as listed in Table 2. As the duty cycle increases in the range from 10 to 20%, the coating porosity first increases and then decreases. In general, the surface porosity depends on the number and diameter of pores. To evaluate the effect of the duty cycle on MAO coating, the number distribution of micro-pores with various sizes should be considered comprehensively. Fig. 4 shows that a large number of pores are distributed all over the surfaces.

For the high duty cycles (15 and 20%), the number of fine pores (< 2 μm) is less than 8% and 10% duty cycles. Moreover, the coating with 15% duty cycle has more pores with the size of > 5 μm, which resulted in the high surface porosity. However, the surface porosity of the coating with 20% duty cycle is low due to the small number of micro-pores with fine and large size. Erfanifar et al. [27] indicated that increasing discharge energy could decrease the surface porosity. The high discharge energy made molten alumina flow out through the discharge channels. The alumina flowed out of the channel and rapidly solidified by the electrolyte, forming the pancake kind of structure (Fig. 3(d)) [28,29]. Sundararajan et al. [28] revealed the product of term $N_c V_p$ was nearly a constant (C) independent of the MAO time. N_c was the number of the discharge channels; V_p was the volume of the pancake, which was defined as follows:

$$V_p = (\pi/8) d_p^2 d_c \tag{3}$$

where d_p is the pancake diameter; dc is the channel diameter.

Thus,

$$N_c d_p^2 d_c = C \tag{4}$$

The product of the term $N_c d_c$ reflected the magnitude of the coating surface porosity.

The Eq. (4) indicated the presence of the pancakes can decrease the porosity of the MAO film with the 20% duty cycle. Besides, the pores with lager size dc increases, which led to the decrease in the number Nc. Consequently, the coatings with the 15% duty cycle had less number of discharge channels. On the other hand, the enlarged images of Fig. 3(c) and (d) show that intersecting slits are formed on the coating surface (marked by ellipse). These slits can play the role of stress concentrators on cyclic stress load [7]. Moreover, all coatings exhibit the existence of cracks (marked by arrow). The presence of these cracks and slits may be associated with thermal stress production and relaxation or release of high-pressure oxygen gas during coating

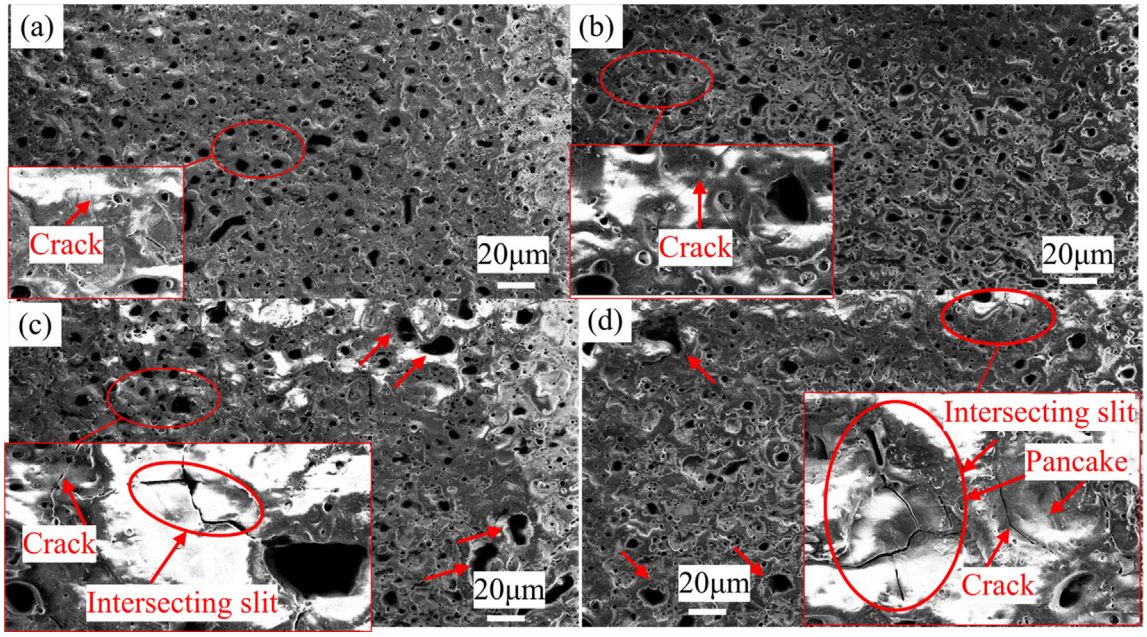

Fig. 3. SEM images of the oxides for (a) 8%, (b) 10%, (c) 15%, and (d) 20%.

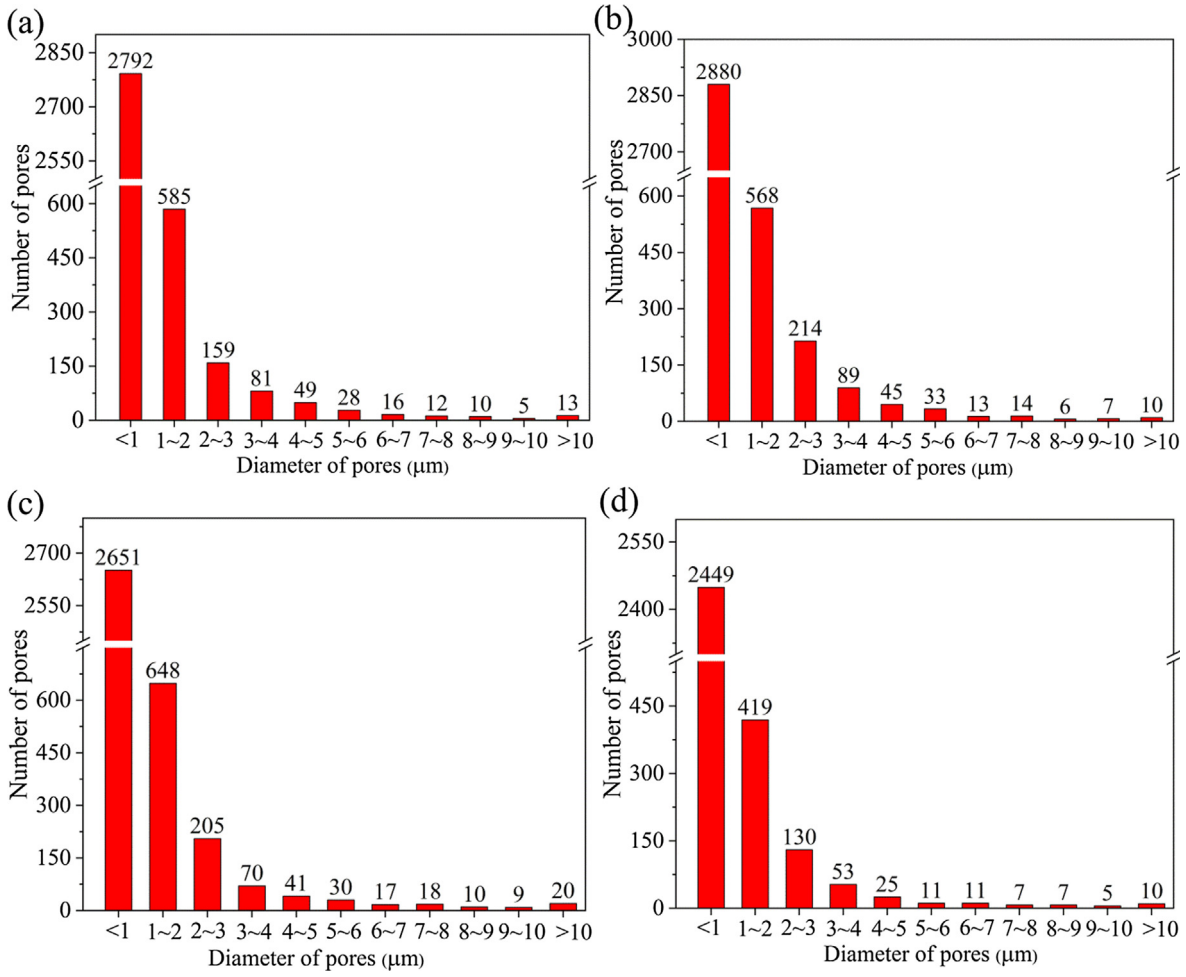

Fig. 4. Distribution of pores in MAO coatings: (a) 8%, (b) 10%, (c) 15%, and (d) 20%.

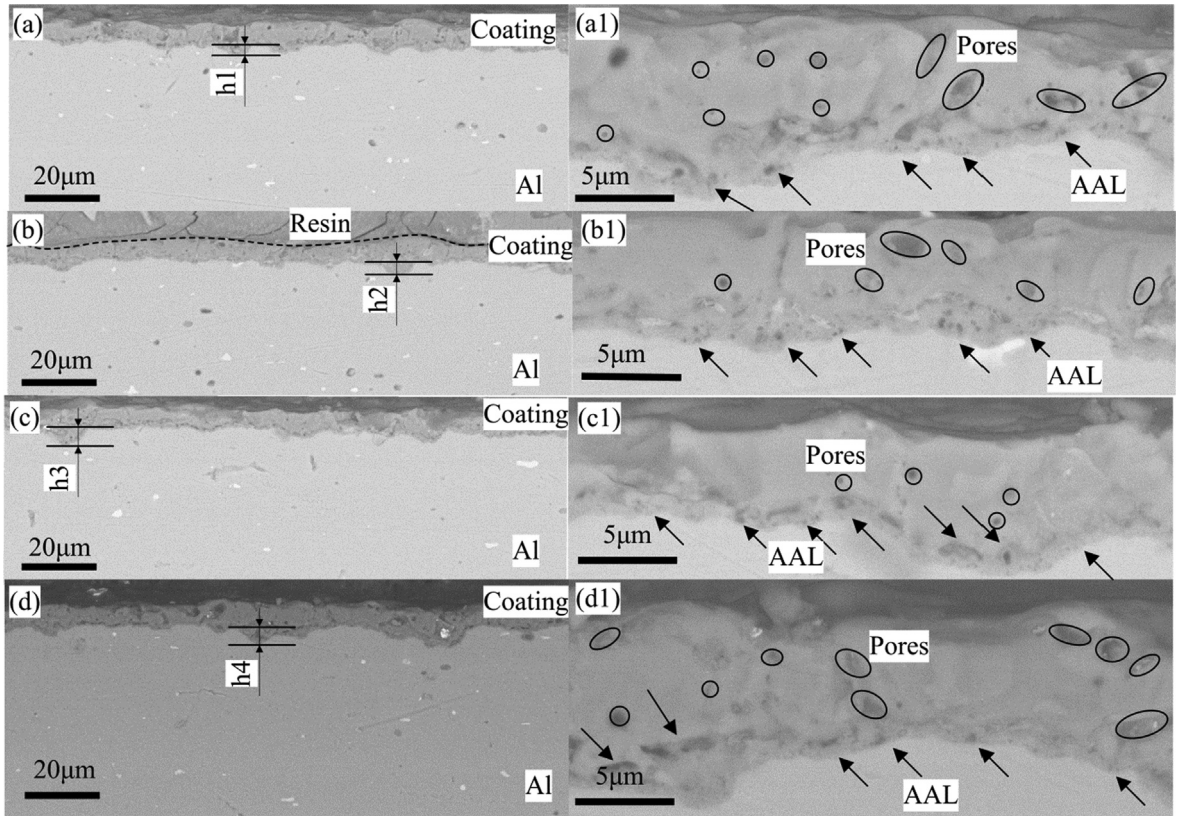

Fig. 5. SEM images of the cross-sections of the oxide layers for (a), (a1) 8%; (b), (b1) 10%; (c), (c1) 15%; (d), (d1) 20%.

formation [30]. With the duty cycles of 15 and 20%, the coatings had cracks with larger size due to the larger discharge energy and the rapid cooling of molten alumina. Moreover, the pancakes are displayed in the MAO coating with the 20% duty cycle. Therefore, the surface roughness of the ceramic layers with high duty cycles is higher than that with low duty cycles (Table 2). In addition, the elastic modulus of coated samples increased compared to that of bare Al alloy (Table 2) due to the high strength of the interface bonding and the coating lacking ductility.

SEM micrographs of the cross-section of the coated samples are shown in Fig. 5. These results indicate that interface between coating and substrate is not smooth as shown in Fig. 5(a) and (b). This particular morphology of the interface was not caused by excessive growth of the coating into the substrate during the MAO process, rather the surface of the substrate itself was rougher (Ra = 0.8). The interface is inclined to be rather zigzag. Maximum height difference from the lower surface of the coating to the upper surface of the substrate is expressed by *h*. The value of *h* is 2.86, 2.86, 5.14, and 4.86 μm, respectively. Compared to duty cycles of 8 and 10%, the coating with the duty cycles of 15 and 20% exhibits a slight growth into the substrate. This phenomenon can be explained by the mechanism of the coating growth. The amorphous alumina layer (AAL, marked by arrow) covering the substrate is the active zone for the formation of molten alumina [31,32]. The AAL was is mainly porous continuous alumina. Many researchers had investigated the morphologies by TEM and detached technology [32,33]. The substrate had valleys and peaks in its surface due to roughness. The coating was prone to forming at the valleys due to the sharp-angled effect [34,35]. The enormous energy input melted the substrate significantly. Subsequently, a lot of the molten alumina flowed out of the discharge channel and attached to the substrate.

Therefore, the oxide film grows inwards to the AA7075-T6 alloy substrate and outwards to the MAO coating surface simultaneously, which is consistent with the literature report [36].

Moreover, no penetrating cracks and pores are found in the cross-section of the coatings. The pores may be caused by the molten alumina into other discharge channels and not through entire the coatings [37]. Troughton et al. [38] also found this phenomenon.

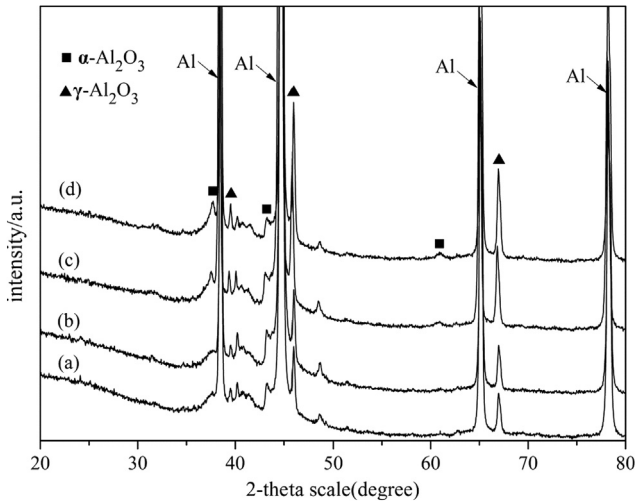

Fig. 6. XRD patterns of MAO coatings for (a) 8%, (b) 10%, (c) 15%, and (d) 20%.

The XRD patterns of the coatings deposited on AA7075-T6 alloy are shown in Fig. 6. Based on the peak analysis, the relative intensity of peaks corresponding to γ-Al_2O_3 increases slightly with increasing duty cycle, indicating a slight increase in the content of γ-Al_2O_3 and α-Al_2O_3 phases [39]. γ-Al_2O_3 phase was easily produced at faster cooling rates [40]. The low temperature electrolyte medium cooled the molten alumina rapidly and the coating was formed around the discharge channels. The coating thickness with 15 and 20% duty cycles was thick. Thus, the content of γ-Al_2O_3 was high. Owing to thinner coating and better heat dissipation conditions, less α-Al_2O_3 is formed in the internal

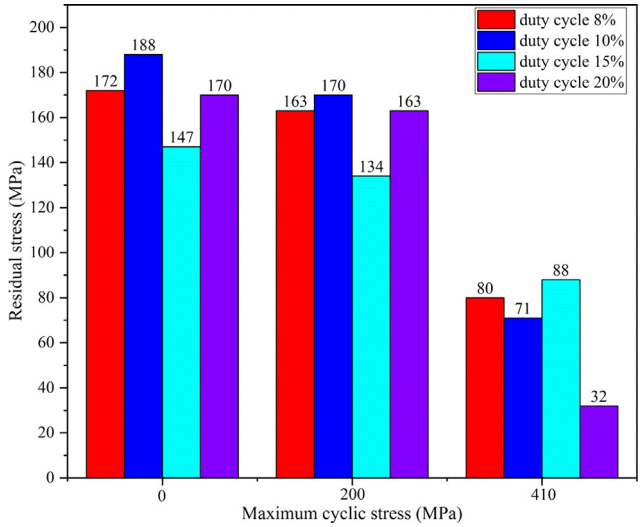

Fig. 7. The residual stress of coated specimens treated using different duty cycles.

layer [41].

In previous work, the coating growth was considered to be an ejecting process of molten alumina, which may be induced high content of α-Al_2O_3. Zhu and his worker proposed a new mechanism of coating growth [32]. The growth mechanism can reasonably reveal the presence of less content of α-Al_2O_3 and the AAL. On the other hand, a large amount of heat was generated around the discharge channels with large size (Fig. 4), which converted a small amount of γ-Al_2O_3 into α-Al_2O_3. In addition, since thermal expansion coefficient of the coating oxide is different from that of Al alloy substrate, the content of oxide layers significantly affects the fatigue behavior of the substrate [30,42]. However, the signs of the residual stress are not affected by the coating content completely because MAO treatment involves complex chemical reactions and heat exchange [1,43]. In general, pores are the prerequisite of the MAO treatment [32], which made the distribution of the residual stress more complicated.

3.2. Mechanism of the residual stress relaxation in the coating

Fig. 7 shows the magnitude of residual stress existing in the coatings with different duty cycles. The residual stress is tensile stress. Moreover, the mean magnitude of the tensile stress decreased at 15% duty cycle. Since the slits and many pores with large size were found on the coatings with the 15 duty cycle, the tensile stress was released. In addition, pores were essential to reducing the magnitude of the residual stress [44]. Therefore, the interface between the coating and substrate was not impaired by the high magnitude of residual stress due to mismatch strain [45]. However, the nature of residual stress in MAO coating was rarely discussed. Lonyuk et al. [7] determined the residual compressive stress in the MAO coatings which mainly consisted γ-Al_2O_3 deposited on 7475-T6 Al alloy. However, Kong et al. [46] acquired 8, 15, and 20 μm MAO coating on 7475 Al alloy surface and the residual tensile stress were 127 MPa, 209 MPa, and 318 MPa, respectively. According to this experimental result, the residual stress does not depend on the oxide composition of the coating. Fattough et al. [47] also indicated that the residual stress was caused by the synergistic influence of many factors. For the residual stress caused by the mismatch strain, Freund and his worker give the calculation formula, as shown in Eq. (5) [48].

$$\sigma_m = \in_m M_C \tag{5}$$

where M_C and $\in_m$ are biaxial elastic modulus, the mismatch strain. Corresponding calculation formula are Eqs. (6) and (7), respectively.

$$M_C = \frac{E}{1-\nu} \tag{6}$$

where E is the Young's modulus of the MAO coating; ν is the Poisson's ratio of the ceramic layer.

$$\in_m = \alpha_C(T_C - T_0) - \alpha_S(T_S - T_0) \tag{7}$$

where α_C (10^{-6}/℃) and T_C ($20 \le T_C \le 1627$) are the thermal expansion coefficient and the temperature of the coating, respectively; α_S (10^{-6}/℃) and T_S ($27 \le T_S \le 627$) are the thermal expansion coefficient and the temperature of the Al alloy substrate, respectively; T_0 is related to the temperature of the electrolyte.

Thus, the Eq. (5) can be written as follows:

$$\sigma_m = \frac{E}{1-\nu}(\alpha_C T_C - \alpha_S T_S + \alpha_S T_0 - \alpha_C T_0) \tag{8}$$

As the thermal expansion coefficient of the substrate (α_S) is four times that of alumina (α_C) [49], the nature of the residual stress (σ_m) was determined by the signs of $\alpha_C T_C - \alpha_S T_S$. The Eq. (8) indicated that the nature of the residual stress in MAO coating was affected by the thermal expansion coefficient and temperature gradient between the substrate and the ceramic coating.

It is interesting to note that the magnitude of the residual stress in MAO coating decrease as the cyclic maximum stress increases. The results show that the residual stress relaxation not only exists in plastic materials, but also presents in MAO coatings. Moreover, the effect of the external stress on the residual stress relaxation in ceramic layer was consistent with that in the shot-peened medium-carbon steel [50]. At the low cyclic stress (200 MPa), the maximum amplitude of the residual stress reduction is 9.7%. In contrast, the amplitude of the residual stress reduction is 40.13%, even 81.18% under high cyclic loading condition (410 MPa). Curran et al. [43] revealed a moderate temperature change of 200 K expecting to generate a misfit strain of about 3 millistrain could produce in-plane stress of 1 GPa in the MAO coating.

Without the pores and cracks in MAO coating, spallation occurred when the coating was subjected to thermal shock [43]. Moreover, studies revealed that the coated sample had excellent thermal shock resistance [51,52]. The morphologies of the MAO coating with the 20% duty cycle was measured using a 3D measuring laser microscope (LEXT OLS4100) before and after fatigue test, as shown in Fig. 8. As the residual tensile stress was produced in MAO coating, the thermal deformation of the coating was larger than that of the substrate (Eq. (8)). The decrease of the residual stress should be attributed to the decrease of the mismatch strain between the substrate and the coating. In Fig. 8, numerous cracks in the coating surface are closed after fatigue test (marked by arrow). Moreover, a few micro-pores disappear. Thus, the thermal deformation of the coating decreased, which is the crucial reason of the residual stress relaxation. However, new crack appeared in the layer after fatigue test (marked by elliptic). This may be caused by the loss of the pore, which redistributed the stress around the discharge channel and achieved local equilibrium. In addition, the magnitude of the decrease in mismatch strain due to the tensile cyclic loading can be obtained by Eq. (5).

For the 20% duty cycle, the residual tensile stress in the coating decreased by 138 MPa at S_{max} = 410 MPa compared to the sample without fatigue test. The corresponding amplitude of $\in_m$ was 4.145×10^{-4}, where E and ν of the MAO coating was 253 GPa and 0.24, respectively. The presence of pores and cracks on the MAO treated surface is likely to cause the reduction in mismatch strain. On the other hand, the strain of the bare substrate and coated samples treated with the 20% duty cycle was measured using an extensometer. Compared with bare AA7075-T6 alloy, the strain change amplitude of the coated specimen is 0.003% and 0.093% at S_{max} = 200 and 410 MPa for 2000 cycles, respectively. Under the high cyclic stress (410 MPa), the coatings affected the strain of the substrate significantly. The MAO coating exhibited excellent adhesive strength to the substrate [49]. Thus, large elastic deformation of the substrate at S_{max} = 410 MPa led to the crack

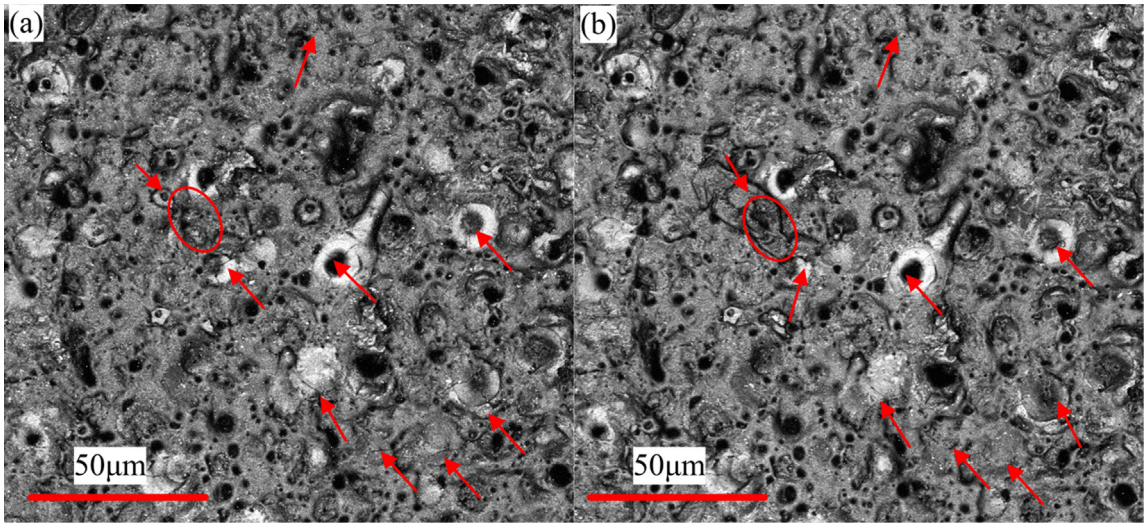

Fig. 8. The morphologies of the MAO coating with the 20% duty cycle (a) without fatigue test, (b) after fatigue test.

closure, mismatch strain reduction, and residual stress relaxation. In addition, the residual stress relaxation of 310 MPa may be produced by the 0.093% strain change caused by the coating (Eq. (5)). However, the 0.003% strain change only can produce 10 MPa residual stress relaxation. In sum, from the theoretical calculation of mismatch strain and stress as well as the observation of the coating surface, the formation mechanism and relaxation of the residual stress in the MAO layers is reasonable. However, the study only discusses the formation mechanism of the residual stress, and its prediction model needs to be further explored since the coating pores and cracks cause a large difference in elastic modulus and thermal expansion coefficient [43]. Moreover, the pores and cracks resulted in the theoretical magnitude of the residual stress relaxation (310 MPa) greater than the measured value (138 MPa).

3.3. Fatigue studies of coated samples

Fatigue life of the bare Al alloy and the coated specimens processed for different duty cycles are presented in Fig. 9. At each stress level, parallel tests were performed on three or four samples. As shown in Fig. 9, the S-N curves were obtained by the least squares method. The detail of fatigue data treatment was introduced in our previous work [53]. In general, the fatigue life of the coated samples is lower than that

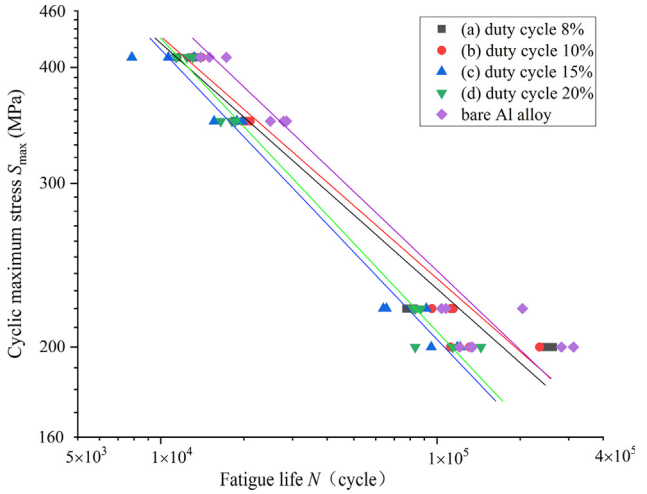

Fig. 9. Fatigue lives of bare specimens and coated specimens for (a) 8%, (b) 10%, (c) 15%, and (d) 20%.

of bare Al alloy at the four stress levels. Moreover, the fatigue life of the bare AA7075-T6 alloy is more dispersive than that of coated Al alloy at the low cyclic stress. Schijve also indicated the same issue about the dispersion of fatigue life [54]. On the one hand, lattice rotation occurred in AA7075-T6 alloy during crack propagation, which constantly altered fatigue parameters [55]. Previous study showed that two types of second phase particle presented in AA7075 alloy substrate [56].

Moreover, crack initiated in the second phase particles [57]. These factors lead to a large dispersion of the fatigue life. For the coated samples, defects (Fig. 3) easily produced stress concentration and crack initiated at the coating surface. Since the ceramic coating lacked ductility, the coatings can restrain the deformation of the substrate [18]. This was also the reason why the coating was prone to producing cracks in the film formation. Furthermore, residual tensile stress was produced in the ceramic coating. The above factors are attributed to the decrease of the substrate after MAO treatment with different duty cycles. However, the coatings with the duty cycles of 8 and 10% did not seriously impair the fatigue performance of the AA7075-T6 alloy. In general, cracks initiated in the ceramic coatings and propagated to the interface between the coating and the substrate quickly [58]. Meanwhile, the adhesive property between the substrate and coating was excellent, which caused the crack not to grow along the interface. Besides, the path of the crack propagation would insignificantly deflect because the coating was not prone to local yield. This can be seen from the SEM images of the crack propagation in previous studies [13,59]. According to above analysis, the fatigue behavior of the coated samples with cracks on its surface became inferior seriously. However, the results of the fatigue test indicated the crack was inhibited when it reached the interface and did not propagate directly to the substrate. Furthermore, the porous continuous AAL was observed in the SEM images of the cross-section morphology (Fig. (5)). The presence of the pores made the crack tip blunt, as shown in Fig. 10. Unlike the discharge channels on the coating surface, the size of the pores in the AAL is in the nanometer scale, which has little effect on the local strength. Although the micropores presented within AAL, the adhesive strength between the coating and substrate was not deteriorated. In contrast, the pores and cracks in Fig. 3 weakened the local strength of the coating [60]. Deng et al. [61] found that crack tip blunting increased the fracture toughness of the porous ceramics.

$$\frac{K_{IC,\,blunt}}{K_{IC}} = (1 + \frac{\rho_0}{2r_0})^{1/2} \tag{9}$$

where $K_{IC,\,blunt}$ is the fracture toughness in porous ceramics; K_{IC} is the fracture toughness in dense ceramics; ρ_0 is the root radius of the blunt

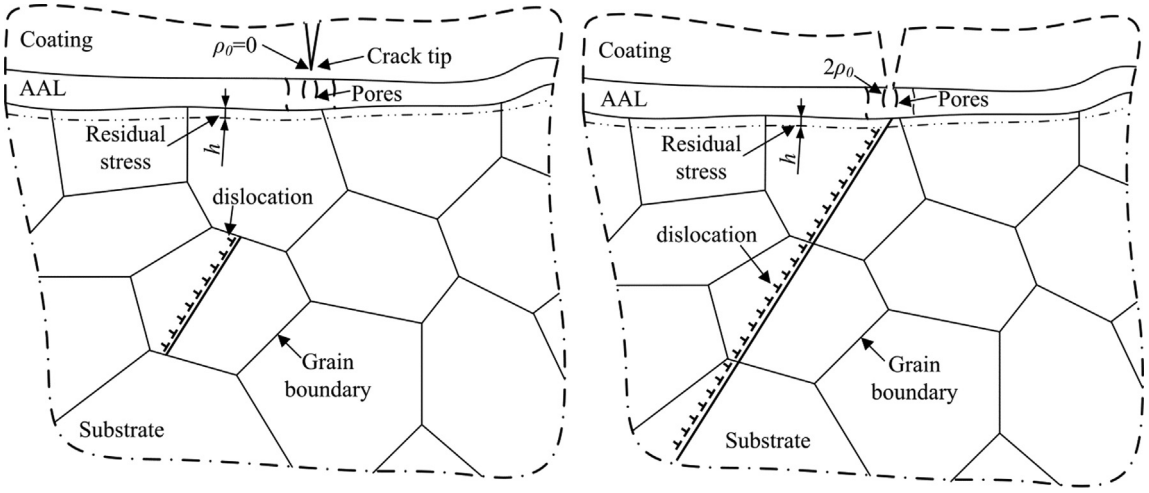

Fig. 10. Schematic diagram of crack tip in MAO coating.

crack; r_0 is the characteristic zone, which can be referred to the literature [61,62]. The increase of the fracture toughness $K_{IC,\ blunt}$ delayed the rate of the crack propagation from the AAL to the AA7075-T6 alloy substrate. Besides, the crack tip blunting reduced the normal stress at the crack tip [63].

The fracture toughness of Al alloy is nearly 14 times that of alumina [64]. Thus, the crack did not pass through the interface directly from the coating to the substrate. However, the fatigue life of the coated samples decreases compared to that of uncoated samples. This was caused by the large opening stress applied to the substrate. The effect of the external loading on the crack tip was shielded within the ceramic coating, while the substrate adjacent to the crack tip was subjected to greater opening stress [65], as shown in Fig. 10. Meanwhile, the dislocations within the substrate were produced and moved along slip plane under the cyclic stress loading [66]. Tanaka et al. [67] proposed an equilibrium condition of dislocations, as shown in Eq. (10).

$$\tau_1^D + \tau_1 - k = 0 \tag{10}$$

where τ_1^D is the dislocation stress (back stress); τ_1 is the external shear stress; k is the frictional stress.

However, the dislocation reached the region of the residual stress and the residual stress should be treated as principal stress [68]. Thus, Eq. (11) is expressed as

$$\tau_1^D + \tau_1 + \tau^R - k = 0 \tag{11}$$

where τ^R is the resistance to dislocation movement caused by the residual stress.

Studies showed that the substrate adjacent to the coating was subjected to the identical amplitude of the residual stress which was produced in the coating; however, the sign was adverse [10,69]. Therefore, the residual stress in the substrate adjacent to the coating is compressive stress in this study, which resulted in stagnation of the dislocations. Notably, the size of the residual stress region (marked h) produced by MAO treatment is much smaller than that by shot peening since the formation of coating was mainly caused by the melting of Al on the surface of the substrate and other areas were not affected due to the rapid cooling of electrolyte [14,70]. Consequently, the dislocation pile-ups presented near the interface. For the prior shot peened MAO (SP + MAO) coated samples, the depth of the residual compressive stress in the substrate can reach 175 μm [14]. Unlike the MAO treatment, the dislocations of the SP + MAO coated specimens did not accumulate adjacent to the interface. The dislocation pile-ups was prone to causing crack initiation and impairing the interface [71]. The effect of residual compressive stress on fatigue performance was quite different for MAO and SP + MAO treatment [11,12]. The impairment of the interface was the crucial issue of the decrease in fatigue life of the MAO coated samples compared to that SP + MAO treatment. Thus, the coating defects and the dislocation pile-ups near the interface were detrimental to fatigue behavior of the substrate.

In addition to dislocation pile-ups, the rate of the crack growth within the coatings [72,73] and the morphology of the interface [14,21] affected the fatigue behavior of the substrate significantly. Fig. 9 shows that the effect of the coating with the 8 and 10% duty cycles at the high and low cyclic stresses was not identical. Under the high cyclic stress loading condition, the fatigue life of the AA7075-T6 alloy was higher than that of the coated samples significantly. In contrast, the impairment of the coating to the fatigue performance of the substrate was alleviated at the low cyclic stress, especially at S_{max} = 200 MPa. Additionally, the fatigue performance of the coated samples treated with 15 and 20% duty cycles was inferior compared to that treated with other duty cycles. Moreover, the fatigue life decreased dramatically at S_{max} = 200 MPa. However, the difference in fatigue life of the coated samples treated with different duty cycles was reduced at the high cyclic stress. Residual tensile stress relaxation and the overgrowth of the coatings (Fig. 5) into the substrate are the crucial issues to the difference in the fatigue performance. At the high cyclic stress, the residual tensile stress in MAO coating decreased significantly at the initial cyclic stress [50], which decreased the residual compressive stress in the substrate. The total number of dislocations N_1 within half size of grain boundary and plastic displacement γ_1 in grain boundary size are determined by Eqs. (12) and (13), respectively [67].

$$N_1 = (\tau_1 + \tau^R - k)a/\pi A \tag{12}$$

$$\gamma_1 = (\tau_1 + \tau^R - k)ba^2/2A \tag{13}$$

where a is the half size of grain boundary; b is the Burgers vector; A is a constant related to the dislocation stress field and determined by Eq. (14).

$$A = Gb/2\pi(1-\nu) \tag{14}$$

where G is the shear modulus, and ν is the Poisson's.

Eqs. (12) and (13) indicated that the number of dislocations N_1 and plastic displacement γ_1 increased under the high loading condition. The decrease of the residual compressive stress within the substrate and the higher applied stress was attributed to the dislocations rapidly moving toward the interface. Subsequently, the dislocations were prone to extrusion. The porous AAL can alleviate the impairment of the stored strain energy of the accumulated dislocations on the interface [67]. Meanwhile, the plastic deformation of the substrate adjacent to the coating was produced accompanied with dislocation motion. This phenomenon can be seen in the fatigue fracture of the coated samples.

Guo et al. [72] systematically studied the relationship between the crack velocity and the depth of the crack in the substrate resulting from the coating cracking. The residual tensile stress and the thick ceramic layers, and the high applied stress would cause the crack growth rate to be faster in the MAO coating, which weakened the fatigue behavior of the substrate significantly [56,72]. Therefore, the fatigue performance of the substrate covered with the ceramic layers was inferior.

As the cyclic stress decreased, both N_1 and γ_1 declined which affected the property of the interface and reduced the number of dislocations transmitted by the dislocation source. The effect of the back stress produced by the dislocation pile-ups on the property of the interface was alleviated due to the decrease in dislocations at the lower cyclic stress. However, the larger residual compressive stress made the dislocations stagnate near the interface. With the increase of the cycles in fatigue test, the number of dislocations accumulating within the region of the residual compressive stress increased, resulting in higher magnitude of the back stress. For the coated samples treated with the 15 and 20% duty cycles, the combined effects of the overgrowths and dislocation pile-ups near the interface were prone to originating cracks [73]. Consequently, the interface was impaired significantly and the fatigue crack initiating from the MAO layer can propagate through the interface into the AA7075-T6 alloy, causing a remarkable decrease in its fatigue life. However, the coating with 8 and 10% duty cycles did not show significant overgrowth near the interface and premature cracks were not produced. Moreover, the size of the cracks on the coating was small and the coating thickness was thin. Under the lower cyclic stress loading condition, the crack depth of the AA7075-T6 alloy substrate was small. Increasing the back stress was likely to make the dislocation move toward the interface as fatigue tests proceed (Eq. (11)). Finally, the dislocations were extruded. The surface of the plastic zone should rough because of the start and stop of dislocation in the morphology of the fatigue fracture. Thus, the fatigue performance with the 8 and 10% duty cycles was impaired insignificant. In addition, the coatings with 15 and 20% duty cycles were thicker than that with 8 and 10% duty cycles. Moreover, high surface porosity and lots of pores with large size were exhibited in the coating with the 15% duty cycle. These defects caused premature cracking of the coatings. The fatigue property was worse than that of the coated samples treated with the 8 and 10% duty cycles at all cyclic stresses.

Fig. 11 shows the fatigue fracture of bare and coated samples at S_{max} = 220 MPa. Enlarged view of the crack initiation for the 20% duty cycle was inspected at S_{max} = 220 and 410 MPa, respectively. Fig. 11(a-e) clearly show crack initiation, propagation, and fatigue rupture regions. The fatigue fracture presents a radial surface topography, which is typical characteristic of fatigue fracture morphology of specimen with rectangular section [54]. Since the constraints on cyclic plasticity were minimal, fatigue cracks were produced at the corners of the rectangular section. Before MAO treatment, surface roughness of bare Al alloy was Ra = 0.8 and two types of second phase particles presented in substrate. Cracks were easily formed in defects. Therefore, the crack initiation did not occur at the corners. However, the bonding strength of coating and substrate was higher and oxide film had poor ductility. Wang et al. [74] indicated the thickness was thick at the edges than that at the center due to the sharp-angled effect. The corners of the rectangular section easily caused crack initiation. Moreover, microstructure of the coating and the substrate after the fracture of the failed specimen is shown in Fig. 11(f) and (h). Larger pores on the coating and penetrating crack are observed in the crack initiation, as shown in Fig. 11(f). Furthermore, a micro-pore presents in the front of the crack. These characteristics coincide with the model of the impaired substrate induced by coating cracking. In addition, the size of local plastic deformation zone (marked by arrows with the dotted line) of the substrate adjacent to the coating at S_{max} = 220 MPa is lower than that at S_{max} = 410 MPa. Moreover, Fig. 11(f) shows that slip lines presented within the plastic deformation zone. The direction of the plastic deformation zone is inclined to the surface of the samples, which is consistent with the characteristics of plastic deformation caused by shear force. Besides, the surface of fatigue fracture adjacent to the coating (marked by the ellipse with the dotted line) is rough. At the lower cyclic stress loading condition, the dislocations may stagnate near the interface and moved again under the larger back stress. Moreover, the second phase particles existed in AA7075-T6 alloy. Thus, the plastic zone exhibits the appearance of the steps and the coarse surface (marked by the ellipse). In contrast, the dislocations can propagate smoothly from the substrate to the interface and did not stop near the interface at S_{max} = 410 MPa. Thus, the plastic deformation region is long and presents a smooth surface morphology adjacent to the interface. In previous studies, the apparent plastic deformation due to slip was not observed in the SEM images of the fracture surface near the coating of SP + MAO coated specimen [14]. Moreover, the crack deflected significantly when the crack grew out of the residual compressive stress zone [11,12]. This resulted from the residual compressive stress with high depth in the substrate inhibiting the local plastic deformation. The above results are consistent with the analysis of the residual stress relaxation on the fatigue property. Notably, Fig. 11(h) shows intergranular fracture of the coating which was produced by the high cyclic stress and the extrusion of dislocations [72,73]. In Fig. 11(g), a crack with large size caused by coating cracking is found. The direction of the crack propagating is close to the glide plane and the crack deflected significantly. SEM images of the fatigue crack progression in plain MAO coated Al alloys exhibited similar phenomenon in literature [13]. In addition, crack growth region of the coated specimen is different from that of the uncoated specimen. The crack propagation length in the Y-axis direction was unchanged. However, the propagation length in the X-axis direction of coated samples was significantly greater than that of bare Al alloy. This was attributed to the residual stress, which changed crack propagation path. However, fatigue cracks propagated adjacent to coatings. Residual compressive stress was related to the distance between the substrate and the interface [17,53]. Defects and residual tensile stress existed in MAO coatings. The change in fatigue crack propagation path was disadvantageous to the fatigue performances of coated samples.

4. Conclusions

(1) Duty cycles affected the size of pores and cracks in MAO coating. Larger intersecting slits and less fine pores were presented in the ceramic layers with the 15 and 20% duty cycles compared to that with the duty cycles of 8 and 10%. Moreover, surface porosity of the coating with 15% duty cycle was relatively high and more pores with the size of > 5 μm was produced in the coating surface. Besides, the formation of pancakes in the MAO film with the 20% duty cycle results in low surface porosity.

(2) The overgrowth of the coating into the substrate was found in the thin films. The coating was prone to forming in valleys due to the substrates' roughness. High discharge energy using the 15 and 20% duty cycles caused the production of the overgrowth.

(3) Residual tensile stress relaxation in MAO coating was attributed to the pores and cracks. At high cyclic stress, the relaxation of residual tensile stress was dramatic and dislocation pile-ups adjacent to the interface were eliminated. Meanwhile, crack closure appeared and a small number of discharge channels on the coating surface disappeared. In contrast, the residual tensile stress decreased insignificantly at low cyclic stress, which resulted in the dislocation accumulation near the interface.

(4) Crack tip blunt and residual stress relaxation affected the fatigue behavior of the coated samples. The crack tip blunting prevented the crack passing through the interface directly from the amorphous alumina layer to the substrate. Thus, the MAO coating did not seriously impair the fatigue performance of the substrate. However, the fatigue behavior of the samples treated with the 15 and 20% duty cycles was inferior compared to 8 and 10% duty cycles under

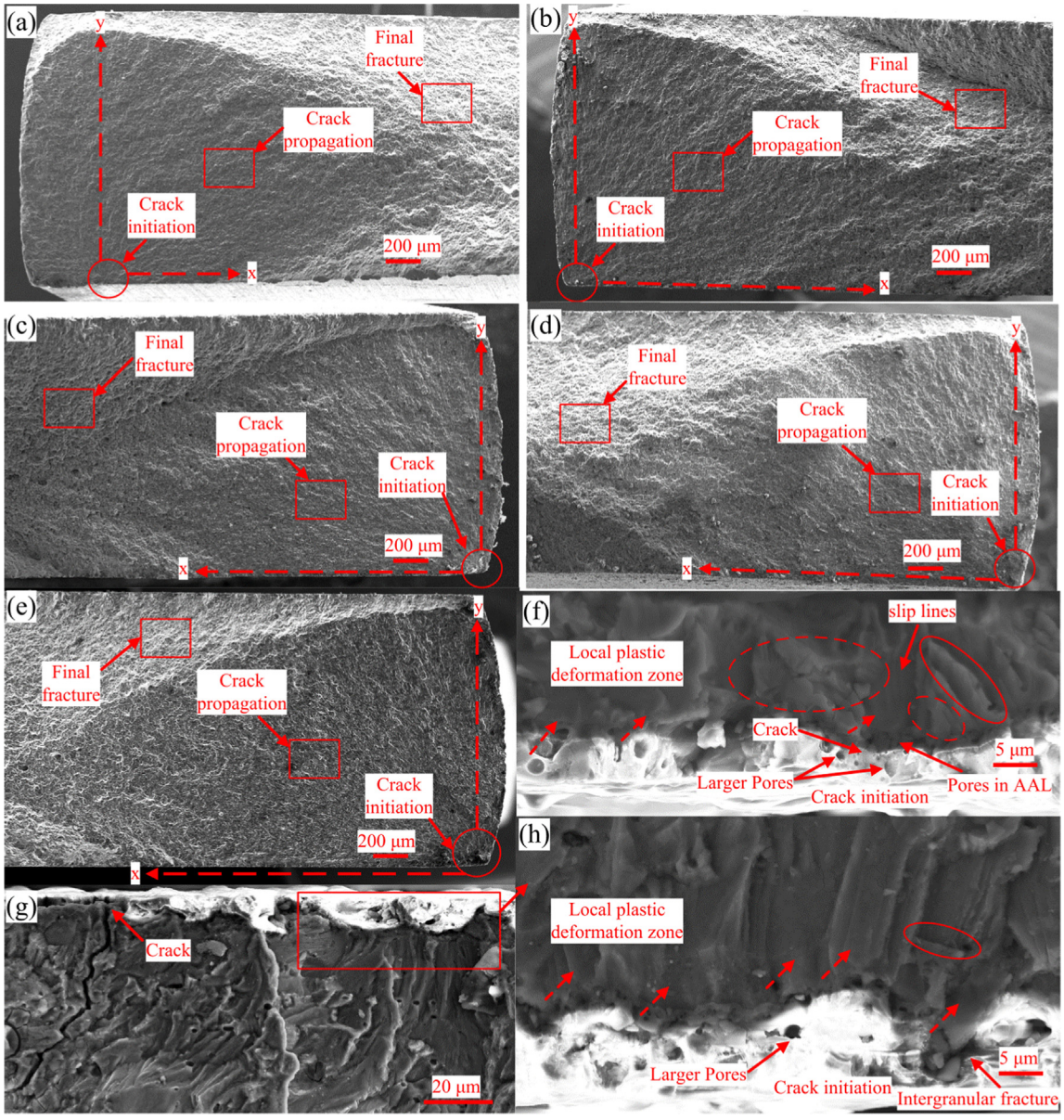

Fig. 11. Fatigue fracture of the bare and coated samples at S_{max} = 220 MPa:(a) bare, (b) 8%, (c) 10%, (d) 15%, (e) 20%, (f) and (g) – (h) were an enlarged view of crack initiation for the 20% duty cycle at S_{max} = 220 and 410 MPa, respectively.

the low cyclic stress. The lower fatigue life was attributed to the combined effects of the stress concentration caused by the over-growth and the dislocation pile-ups. At the high cyclic stress, the residual tensile stress relaxation alleviated the impairment of the interface. Thus, the fatigue life with different duty cycles changed insignificantly. In addition, the defects on coating surface including pores and cracks decreased the fatigue life of the substrate.

Acknowledgement

The work was supported by the National Natural Science Foundation of China (Grant Nos. 51575095, 51675089, and U1708254), and China Postdoctoral Science Foundation (2017M610180). Thanks to the Institute of Aeronautics and Astronautics of Tsinghua University for their support in residual stress detection.

References

[1] Sankara Narayanan TSN, Park IS, Lee MH. Strategies to improve the corrosion resistance of microarc oxidation (MAO) coated magnesium alloys for degradable implants: Prospects and challenges. Prog Mater Sci 2014;60:1–71.
[2] Kossenko A, Zinigrad M. A universal electrolyte for the plasma electrolytic oxidation of aluminum and magnesium alloys. Mater Des 2015;88:302–9.
[3] He XJ, Zhang XY, Wang X, Qin L. Review of antibacterial activity of titanium-based implants' surfaces fabricated by micro-arc oxidation. Coatings 2017;7:22.
[4] Hudson CM. Effect of stress ratio on fatigue-crack growth in 7075-T6 and 2024-T3 aluminum-alloy specimens, New York; 1969.
[5] Wang QY, Bathias C, Kawagoishi N, Chen Q. Effect of inclusion on subsurface crack initiation and gigacycle fatigue strength. Int J Fatigue 2002;24:1269–74.
[6] Mohedano M, Serdechnova M, Starykevich M, Karpushenkov S, Bouali AC, Ferreira MGS, et al. Active protective PEO coatings on AA2024: Role of voltage on in-situ LDH growth. Mater Des 2017;120:36–46.
[7] Lonyuk B, Apachitei I, Duszczyk J. The effect of oxide coatings on fatigue properties of 7475–T6 aluminium alloy. Surf Coat Technol 2007;201:8688–94.
[8] Rajasekaran B, Raman SGS, Krishna LR, Joshi SV, Sundararajan G. Influence of microarc oxidation and hard anodizing on plain fatigue and fretting fatigue behaviour of Al-Mg-Si alloy. Surf Coat Technol 2008;202:1462–9.
[9] Asquith DT, Yerokhin AL, Yates JR, Matthews A. Effect of combined shot-peening and PEO treatment on fatigue life of 2024 Al alloy. Thin Solid Films 2006;515:1187–91.

[10] Wasekar NP, Ravi N, Babu PS, Krishna LR, Sundararajan G. High-cycle fatigue behavior of microarc oxidation coatings deposited on a 6061–T6 Al alloy. Metall Mater Trans A-Phys Metall Mater Sci 2010;41A:255–65.
[11] Krishna LR, Madhavi Y, Sahithi T, Wasekar NP, Chavan NM, Rao DS. Influence of prior shot peening variables on the fatigue life of micro arc oxidation coated 6061–T6 Al alloy. Int J Fatigue 2018;106:165–74.
[12] Madhavi Y, Krishna LR, Narasaiah N. Influence of micro arc oxidation coating thickness and prior shot peening on the fatigue behavior of 6061–T6 Al alloy. Int J Fatigue 2019;126:297–305.
[13] Krishna LR, Madhavi Y, Sahithi T, Rao DS, Ijeri VS, Prakash O, et al. Enhancing the high cycle fatigue life of high strength aluminum alloys for aerospace applications. Fatigue Fract Eng Mater Struct 2019;42:698–709.
[14] Ye Z, Liu D, Zhang X, Wu Z, Long F. Influence of combined shot peening and PEO treatment on corrosion fatigue behavior of 7A85 aluminum alloy. Appl Surf Sci 2019;486:72–9.
[15] Sundararajan G, Wasekar NP, Ravi N. The influence of the coating technique on the high cycle fatigue life of alumina coated Al 6061 alloy. Trans Indian Inst Met 2010;63:203–8.
[16] Wang YM, Zhang PF, Guo LX, Ouyang JH, Zhou Y, Jia DC. Effect of microarc oxidation coating on fatigue performance of Ti-Al-Zr alloy. Appl Surf Sci 2009;255:8616–23.
[17] Ao N, Liu D, Zhang X, Liu C. Enhanced fatigue performance of modified plasma electrolytic oxidation coated Ti-6Al-4V alloy: Effect of residual stress and gradient nanostructure. Appl Surf Sci 2019;489:595–607.
[18] Leoni A, Apachitei I, Riemslag AC, Fratila-Apachitei LE, Duszczyk J. In vitro fatigue behavior of surface oxidized Ti35Zr10Nb biomedical alloy. Mater Sci Eng C-Mater Biol Appl 2011;31:1779–83.
[19] Wang XS, Guo XW, Li XD, Ge DY. Improvement on the fatigue performance of 2024–T4 alloy by synergistic coating technology. Materials 2014;7:3533–46.
[20] Yang HH, Wang XS, Wang YM, Wang YL, Zhang ZH. Microarc oxidation coating combined with surface pore-sealing treatment enhances corrosion fatigue performance of 7075–T7351 Al alloy in different media. Materials 2017;10.
[21] Dai WB, Yuan LX, Li CY, He D, Jia DW, Zhang YM. The effect of surface roughness of the substrate on fatigue life of coated aluminum alloy by micro-arc oxidation. J Alloy Compd 2018;765:1018–25.
[22] Weng HF, Chen QL, Cai X, Bao MD. Effects of pulse duty cycles on microarc oxidation formed on Al. Surf Technol 2005;34:59–62.
[23] Arunnellaiappan T, Babu NK, Krishna LR, Rameshbabu N. Influence of frequency and duty cycle on microstructure of plasma electrolytic oxidized AA7075 and the correlation to its corrosion behavior. Surf Coat Technol 2015;280:136–47.
[24] Dehnavi V, Luan BL, Shoesmith DW, Liu XY, Rohani S. Effect of duty cycle and applied current frequency on plasma electrolytic oxidation (PEO) coating growth behavior. Surf Coat Technol 2013;226:100–7.
[25] Zhang J, Fan Y, Zhao X, Ma R, Du A, Cao X. Influence of duty cycle on the growth behavior and wear resistance of micro arc oxidation coatings on hot dip aluminized cast iron. Surf Coat Technol 2018;337:141–9.
[26] Nomine A, Nomine AV, Braithwaite NSJ, Belmonte T, Henrion G. High-frequency-induced cathodic breakdown during plasma electrolytic oxidation. Phys Rev Appl 2017;8.
[27] Erfanifar E, Aliofkhazraei M, Nabavi HF, Rouhaghdam AS. Growth kinetics and morphology of microarc oxidation coating on titanium. Surf Coat Technol 2017;315:567–76.
[28] Sundararajan G, Krishna LR. Mechanisms underlying the formation of thick alumina coatings through the MAO coating technology. Surf Coat Technol 2003;167:269–77.
[29] Jaspard-Mecuson F, Czerwiec T, Henrion G, Belmonte T, Dujardin L, Viola A, et al. Tailored aluminium oxide layers by bipolar current adjustment in the Plasma Electrolytic Oxidation (PEO) process. Surf Coat Technol 2007;201:8677–82.
[30] Apachitei I, Lonyuk B, Fratila-Apachitei LE, Zhou J, Duszczyk J. Fatigue response of porous coated titanium biomedical alloys. Scr Mater 2009;61:113–6.
[31] Rogov AB, Yerokhin A, Matthews A. The role of cathodic current in plasma electrolytic oxidation of aluminum: phenomenological concepts of the “soft sparking” mode. Langmuir 2017;33:11059–69.
[32] Zhu L, Guo Z, Zhang Y, Li Z, Sui M. A mechanism for the growth of a plasma electrolytic oxide coating on Al. Electrochim Acta 2016;208:296–303.
[33] Wang D, Liu X, Wu Y, Han H, Yang Z, Su Y, et al. Evolution process of the plasma electrolytic oxidation (PEO) coating formed on aluminum in an alkaline sodium hexametaphosphate ($(NaPO_3)_6$) electrolyte. J Alloy Compd 2019;798:129–43.
[34] Wei X, Huang H, Sun M, Liu W, Qiu J. Effects of honeycomb pretreatment on MAO coating fabricated on aluminum. Surf Coat Technol 2019;363:265–72.
[35] Wang J, Huang S, He M, Wangyang P, Lu Y, Huang H, et al. Microstructural characteristic, outward-inward growth behavior and formation mechanism of MAO ceramic coating on the surface of ADC12 Al alloy with micro-groove. Ceram Int 2018;44:7656–62.
[36] Hussein RO, Nie X, Northwood DO. An investigation of ceramic coating growth mechanisms in plasma electrolytic oxidation (PEO) processing. Electrochim Acta 2013;112:111–9.
[37] Clyne TW, Troughton SC. A review of recent work on discharge characteristics during plasma electrolytic oxidation of various metals. Int Mater Rev 2019;64:127–62.
[38] Troughton SC, Nomine A, Dean J, Clyne TW. Effect of individual discharge cascades on the microstructure of plasma electrolytic oxidation coatings. Appl Surf Sci 2016;389:260–9.
[39] Xue WB, Deng ZW, Lai YC, Chen RY. Analysis of phase distribution for ceramic coatings formed by microarc oxidation on aluminum alloy. J Am Ceram Soc 1998;81:1365–8.
[40] Gu WC, Lv GH, Chen H, Chen GL, Feng WR, Yang SZ. Characterisation of ceramic coatings produced by plasma electrolytic oxidation of aluminum alloy. Mater Sci Eng A-Struct Mater Prop Microstruct Process 2007;447:158–62.
[41] Hakimizad A, Raeissi K, Santamaria M, Asghari M. Effects of pulse current mode on plasma electrolytic oxidation of 7075 Al in Na2WO4 containing solution: From unipolar to soft-sparking regime. Electrochim Acta 2018;284:618–29.
[42] Khan RHU, Yerokhin A, Li X, Dong H, Matthews A. Surface characterisation of DC plasma electrolytic oxidation treated 6082 aluminium alloy Effect of current density and electrolyte concentration. Surf Coat Technol 2010;205:1679–88.
[43] Curran JA, Clyne TW. Thermo-physical properties of plasma electrolytic oxide coatings on aluminium. Surf Coat Technol 2005;199:168–76.
[44] Matykina E, Arrabal R, Skeldon P, Thompson GE. Investigation of the growth processes of coatings formed by AC plasma electrolytic oxidation of aluminium. Electrochim Acta 2009;54:6767–78.
[45] Dean J, Gu T, Clyne TW. Evaluation of residual stress levels in plasma electrolytic oxidation coatings using a curvature method. Surf Coat Technol 2015;269:47–53.
[46] Kong DJ, Liu H, Wang JC. Effects of micro arc oxidation on fatigue limits and fracture morphologies of 7475 high strength aluminum alloy. J Alloy Compd 2015;650:393–8.
[47] Fattough M, El-Khabeery MM. Residual stress distribution in burnishing solution treated and aged 7075 aluminium alloy. Int J Mach Tools Manuf 1989;29:153–60.
[48] Freund LB, Suresh S. Thin film materials: stress, defect formation and surface evolution. Boston 2004.
[49] Xin SG, Song LX, Zhao RG, Hu XF. Properties of aluminium oxide coating on aluminium alloy produced by micro-arc oxidation. Surf Coat Technol 2005;199:184–8.
[50] Kim JC, Cheong SK, Noguchi H. Residual stress relaxation and low- and high-cycle fatigue behavior of shot-peened medium-carbon steel. Int J Fatigue 2013;56:114–22.
[51] Shen DJ, Wang YL, Nash P, Xing GZ. Microstructure, temperature estimation and thermal shock resistance of PEO ceramic coatings on aluminum. J Mater Process Technol 2008;205:477–81.
[52] Luo H, Cai Q, He J, Wei B. Preparation and properties of composite ceramic coating containing Al_2O_3-ZrO_2-Y_2O_3 on AZ91D magnesium alloy by plasma electrolytic oxidation. Curr Appl Phys 2009;9:1341–6.
[53] Dai W, Li C, He D, Jia D, Zhang Y, Tan Z. Influence of duty cycle on fatigue life of AA2024 with thin coating fabricated by micro-arc oxidation. Surf Coat Technol 2019;360:347–57.
[54] Schijve J. Fatigue of structures and materials, New York; 2004.
[55] Goswami R, Qadri SB, Pande CS. Fatigue mediated lattice rotation in Al alloys. Acta Mater 2017;129:33–40.
[56] Dai W, Liu Z, Li C, He D, Jia D, Zhang Y, et al. Fatigue life of micro-arc oxidation coated AA2024-T3 and AA7075-T6 alloys. Int J Fatigue 2019;124:493–502.
[57] Xue Y, El Kadiri H, Horstmeyer MF, Jordon JB, Weiland H. Micromechanisms of multistage fatigue crack growth in a high-strength aluminum alloy. Acta Mater 2007;55:1975–84.
[58] McNaney JM, Cannon RM, Ritchie RO. Fracture and fatigue-crack growth along aluminum-alumina interfaces. Acta Mater 1996;44:4713–28.
[59] Winter L, Hockauf K, Lampke T. High cycle fatigue behavior of the severely plastically deformed 6082 aluminum alloy with an anodic and plasma electrolytic oxide coating. Surf Coat Technol 2018;349:576–83.
[60] Leguillon D, Piat R. Fracture of porous materials - Influence of the pore size. Eng Fract Mech 2008;75:1840–53.
[61] Deng ZY, She JH, Inagaki Y, Yang JF, Ohji T, Tanaka Y. Reinforcement by crack-tip blunting in porous ceramics. J Eur Ceram Soc 2004;24:2055–9.
[62] Awaji H, Choi SM, Jayaseelan DD. Indirect estimation of critical frontal process-zone size using a single-edge V-notched-beam technique. J Ceram Soc Jpn 2001;109:591–5.
[63] Zheng X, Hirt MA. Fatigue crack propagation in steels. Eng Fract Mech 1983;18:965–73.
[64] Askeland DR, Phule PP. The science and engineering of materials. Boston 2003.
[65] Sugimura Y, Lim PG, Shih CF, Suresh S. Fracture normal to a bimaterial interface: Effects of plasticity on crack-tip shielding and amplification. Acta Metall Mater 1995;43:1157–69.
[66] Bai Y, Xi Y, Gao K, Yang H, Pang X, Yang X, et al. Brittle coating effects on fatigue cracks behavior in Ti alloys. Int J Fatigue 2019;125:432–9.
[67] Tanaka K, Mura T. A dislocation model for fatigue crack initiation. J Appl Mech 1981;48:97–103.
[68] Withers PJ. Residual stress and its role in failure. Rep Prog Phys 2007;70:2211–64.
[69] Xue WB, Wang C, Li YL, Deng ZW, Chen RY, Zhang TH. Effect of microarc discharge surface treatment on the tensile properties of Al-Cu-Mg alloy. Mater Lett 2002;56:737–43.
[70] Xue WB, Deng ZW, Chen RY, Zhang TH, Ma H. Microstructure and properties of ceramic coatings produced on 2024 aluminum alloy by microarc oxidation. J Mater Sci 2001;36:2615–9.
[71] Zhang P, Zhang ZJ, Li LL, Zhang ZF. Twin boundary: Stronger or weaker interface to resist fatigue cracking? Scr Mater 2012;66:854–9.
[72] Guo T, Qiao L, Pang X, Volinsky AA. Brittle film-induced cracking of ductile substrates. Acta Mater 2015;99:273–80.
[73] Guo T, Chen Y, Cao R, Pang X, He J, Qiao L. Cleavage cracking of ductile-metal substrates induced by brittle coating fracture. Acta Mater 2018;152:77–85.
[74] Wang Y, Jiang Z, Yao Z. Microstructure, bonding strength and thermal shock resistance of ceramic coatings on steels prepared by plasma electrolytic oxidation. Appl Surf Sci 2009;256:650–6.